Novel Structural Changes during Temperature-Induced Self-Assembling and Gelation of PLGA-PEG-PLGA Triblock Copolymer in Aqueous Solutions

Neda Khameh Khorshid, Kaizheng Zhu, Kenneth D. Knudsen, Sara Bekhradnia, Sverre Arne Sande, Bo Nyström*

The thermoresponsive amphiphilic block copolymer poly(D,L-lactic acid-*co*-glycolic acid)-*block*-poly(ethylene glycol)-*block*-poly(D,L-lactic acid-*co*-glycolic acid) (PLGA-PEG$_n$-PLGA), which exhibits a reversible temperature-induced sol–gel transition at higher polymer concentrations in aqueous solution has attached a great deal of interest because of its potential in biomedical applications. In the present work, the length of the hydrophobic PLGA blocks is kept constant, whereas the length of the hydrophilic PEG block is altered and this variation has a pronounced impact on the phase behavior of the aqueous samples and the structure of the polymer. A short PEG block promotes gelation at a low temperature, whereas a longer PEG block shifts the gelation point to higher temperature. By using a combination of turbidity, rheology, and small angle neutron scattering (SANS) methods, the authors have revealed dramatic temperature effects. In dilute solution, the SANS experiments expose asymmetric ellipsoid structures for the copolymer with the short PEG-spacer, whereas spherical core–shell structure is observed for the polymer with long PEG-spacer. In the semidilute concentration regime, SANS measurements disclose similar profiles for the two copolymers. In a broad temperature interval, the transition from spherical core–shell micelles to cylindrical structure and packing of cylinders is observed.

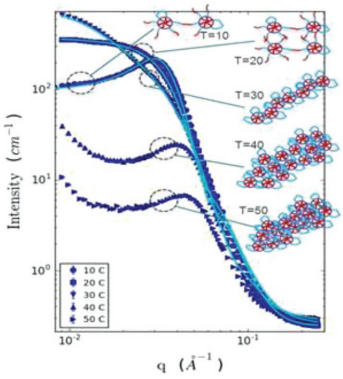

N. K. Khorshid, Dr. K. Zhu, Dr. S. Bekhradnia, Prof. B. Nyström
Department of Chemistry
University of Oslo
P.O. Box 1033, Blindern, N-0315 Oslo, Norway
E-mail: bo.nystrom@kjemi.uio.no
Prof. K. D. Knudsen
Department of Physics
Institute for Energy Technology
P. O. Box 40, N-2027 Kjeller, Norway
Prof. S. A. Sande
School of Pharmacy
Department of Pharmaceutics
University of Oslo
P.O. Box 1068, Blindern, N-0316 Oslo, Norway

1. Introduction

In recent years, amphiphilic block copolymers in which at least one block is thermoresponsive have attracted great interest in the field of self-assembled soft materials.[1–6] Since amphiphilic polymers bear both hydrophobic and hydrophilic groups, they have the potential to self-assemble in water. This process may lead to the formation of thermoreversible hydrogels that can be used as biomaterials for drug delivery and tissue engineering applications.[7–10] Hydrogels are 3D polymeric networks absorbing a significant amount of water. One category of very interesting temperature-induced gelling systems of

DOI: 10.1002/mabi.201600277

great potential for medical applications can be prepared from amphiphilic copolymers of the ABA-type triblock copolymers.

Poloxamers or Pluronics (poly(ethylene oxide)-*block*-poly(propylene oxide)-*block*-poly(ethylene oxide), PEO-PPO-PEO) are classical triblock copolymers in this family that can undergo a temperature-induced reversible sol–gel transition upon heating of an aqueous semidilute solution of the polymer.[11–13] The sol-to-gel transition behavior of Pluronics has been used to deliver instable drugs, such as polypeptides and proteins, since these drugs thereby can be encapsulated at aqueous conditions.[14,15] This formulation can create a gel depot in situ when it is exposed to body temperature via subcutaneous injection. The encapsulated drug may then be released in the body in a controlled manner. The formation of a gel after injection leads to some advantages, such as an injectable matrix that can be implanted in the human body with minimal surgical wounds, and bioactive molecules or cells can be incorporated simply by mixing before injection. However, in spite of the clinical acceptance of Pluronics as solubilizing and thickening agents, these polymers have not met the expectations as pharmaceutical biomedical implants, mostly because of their non-biodegradability and inability to provide sustained drug delivery over long time.[16,17] Actually, the gel depot from PEO-PPO-PEO block copolymers has been found[18] to dissolve from its surface within 1 day into unimers of Pluronics, which due to their ether functional groups resist in vivo degradation[19] and some types may lead to harmful or toxic effects in the body.

Similar to Pluronics, semidilute aqueous solutions of copolymers of the type poly(ethylene glycol)-*block*-DL-lactic acid-*co*-glycolic acid (PEG-PLGA) exhibit sol-to-gel transition as the temperature increases, but in contrast to Pluronics these polymers are biodegradable and the gel state persists for a much longer time both in vitro and in vivo.[20,21] In a previous study of linear poly[(D,L-lactid acid-*co*-glycolic)-*b*-poly(ethylene glycol)-*b*-poly(D,L-lactic acid-*co*-glycolic acid)] (PLGA-PEG-PLGA) copolymer it was reported[21] that the associated physical hydrogel persisted over 3 weeks after subcutaneous injection into rats. PLGA presents some vital advantages compared with Pluronics, e.g., PLGA has hydrolysable ester linkages, which are degraded in the subcutaneous layer of a mammal. In addition, the final degradation products of, e.g., PLGA-PEG-PLGA are lactic acid, glycolic acid, and PEG, which all are approved as safe materials by the United States Food and Drug Administration.

Although many previous studies[22] have established the high potential of PLGA-containing copolymers for the use in biomedical applications, there is a severe lack of investigations dealing with rheological and structural properties of these systems in connection with concentration- and temperature-induced self-assembling and formation of gels of these copolymers in semidilute solutions. To design systems to be applied in, e.g., drug delivery and tissue engineering, it is crucial to have in-depth knowledge of these features, especially the changes of rheological and structural characteristics that take place during the sol-to-gel transition.

In this work, we have studied phase behavior, rheology, and mesoscopic structural properties (using small-angle neutron scattering (SANS)) of $PLGA_{1170}$-PEG_n-$PLGA_{1170}$ triblock copolymer in aqueous solutions. The length of the hydrophobic PLGA blocks was kept constant, whereas the length of the hydrophilic PEG spacer was altered (the number of repeating units $n = 1000$ and 1500). The change of the spacer length will affect the hydrophobicity of the copolymer and this may affect the gelation temperature and the structural features. The aim of this paper is to gain insight into the self-assembling process, and how the mesoscopic structure will be influenced by temperature and spacer in both dilute and semidilute solutions. This work reveals some novel and intriguing structural transitions with temperature, block composition, and polymer concentration. This kind of information is essential in the design of drug carriers and for tissue engineering.

2. Experimental Section

2.1. Materials

D,L-Lactide (LA) and glycolide (GA) from Sigma-Aldrich were recrystallized from ethyl acetate and dried under vacuum and stored at −18 °C before use. Poly(ethylene glycol) (PEG1000 and PEG1500) and stannous 2-ethylhexanoate (stannous octoate, $Sn(Oct)_2$) were purchased from Aldrich-Sigma and used as received without further purification. All other chemicals were reagent-grade and used as purchased.

2.2. Polymer Synthesis

The ABA-type triblock copolymers, PLGA-PEG-PLGA were prepared by ring-opening polymerization (ROP) of D,L-lactide and glycolide with PEG as initiator and stannous octoate as the catalyst.[23,24] Feed ratios of the PEG/GA and LA/GA were used to adjust the composition and molecular weight. The synthetic procedure is outlined below (Figure 1).

The detailed synthesis is conducted in the following way: polyethylene glycol (PEG1000) (15 g, 15 mmol) was dried under dry argon atmosphere in a three-necked flask under vacuum (5 mm Hg) and stirred at 120 °C for 2 h. When the temperature of the flask had decreased to 80 °C, it was back-filled with argon. DL-Lactide (28.4 g, 0.197 mol) and glycolide (7.6 g, 66 mmol) were added in a molar ratio of 3:1, and the reaction mixture was heated under vacuum for another 30 min. After all the DL-lactide and glycolide were melted, 0.02 g of $Sn(Oct)_2$ was added and the reaction mixture was heated to 150 °C and kept there for 12 h.

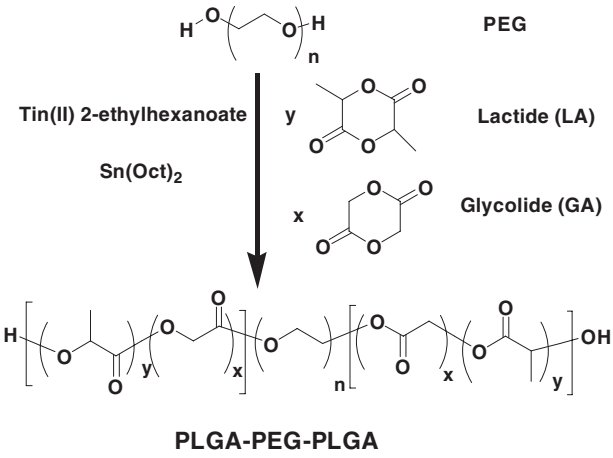

Figure 1. Synthetic route for the preparation of the triblock copolymer PLGA-PEG-PLGA via a ring opening polymerization procedure. The indexes *x*, *y*, and *n* represent the number of repeating units.

The unreacted monomers were removed under vacuum. The flask was then cooled to room temperature, and the residue was dissolved into ice-cold water (4–8 °C). After complete dissolution, the polymer solution was heated to 70–80 °C to induce precipitation of the polymer and to remove water-soluble low-molecular weight polymer and unreacted monomer. Precipitated polymer was isolated by decanting the supernatant and re-dissolving in ice-cold water and heated to induce precipitation. This process of dissolution followed by precipitation was repeated three times. Finally, the polymer was dissolved in a minimum amount of water and lyophilized. The resulting PLGA-PEG-PLGA copolymer was collected and kept at –18 °C.

The chemical structure and composition of the ABA-type triblock copolymers were determined by their ^{1}H NMR spectra in $CDCl_3$ solutions containing tetramethylsilane as reference at 25 °C (Bruker AVANCE DPX 300 MHz spectrometer) (Figure 2). The molar composition of each sample was calculated by comparing the integral area of the PEG methylene signal (5) (δ = 3.65 ppm), the LA single proton (2) (δ = 5.15 ppm), and the GA methylene group (3) (δ = 4.8 ppm). The entire repeating units of LA/GA/EG ($2x/2y/n$) were estimated to be 25/9.46/22 and 24.8/9.54/34 for PEG1000 and PEG1500 derivative polymers, respectively.

Gel Permeation Chromatography (GPC) was performed on a Tosoh Eco-SEC dual detection (RI and UV) GPC system coupled to an external Wyatt Technologies mini-DAWN Treos multi angle light scattering detector. Samples were run in tetrahydrofuran (THF) at a flow rate of 0.5 mL min^{-1} at 35 °C. The column set was one MZ-Gel SD-plus linear column (5 μm, 4.6 × 300 mm). The refractive index increment value (dn/dc = 0.059 mL g^{-1}) was calculated based on the reported dn/dc values of PLGA and PEG in THF (0.054 and 0.068 mg mL^{-1}, respectively).[25,26] Absolute molecular weights and molecular weight

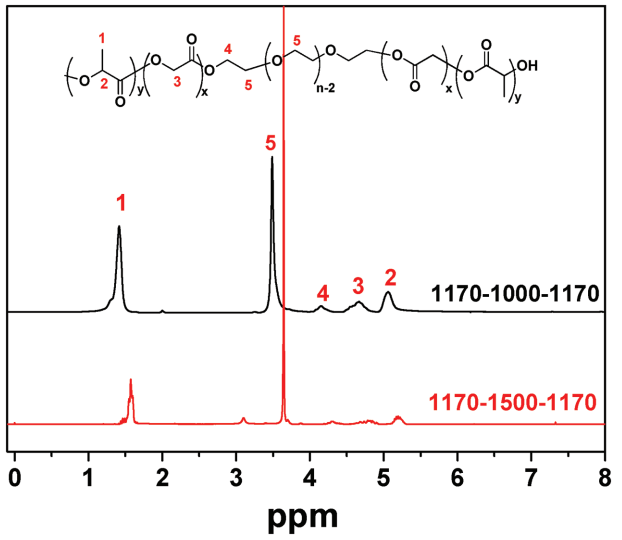

Figure 2. ^{1}H NMR spectra of PLGA-*b*-PEG-*b*-PLGA triblock copolymers ($CDCl_3$-*d* as solvent, 300 MHz).

distribution were calculated using the Astra software package. The polymer sample concentration is 10.0 mg mL^{-1}. Figure 3 shows GPC traces of the resulting copolymers. The elution peaks are symmetric and exhibit no tailing at the lower molecular side. The characteristic data from the synthesis are given in Table 1. In general for many polymer systems, the number-average molar mass (M_n) values determined from GPC are often higher than those determined from NMR because of some minute associations of the polymer in solution that is registered by the light scattering detector.

2.3. Turbidimetry

The cloud point of the solutions was determined via a NK60-CPA cloud point analyzer from Phase Technology. In this approach, phase changes of the sample are registered by a scanning

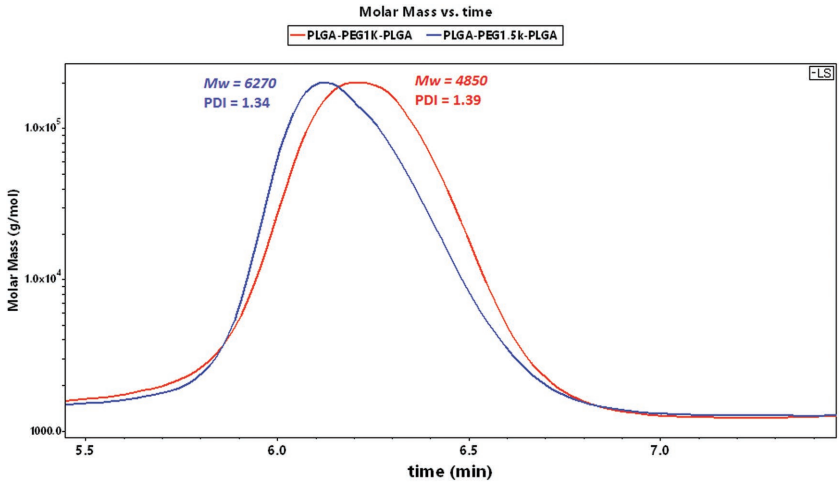

Figure 3. GPC Chromatograms for the two synthesized PLGA-PEG-PLGA triblock copolymers (35 °C, 10 mg mL^{-1} with eluent THF 0.5 mL min^{-1}).

Table 1. Characteristic parameters from the synthesis of PLGA-PEG-PLGA triblock copolymers.

Polymers	PEG (M_n, g mol^{-1})	LA/GA (feed)	LA/GA/EG/GA/LA (*y*/*x*/*n*/*x*/*y*)	M_n (NMR)	M_w/M_n (GPC)
ABA1	1000	2.65 (3)	12.5/4.73/22/4.73/12.5	3340 (1170–1000–1170)	4850/3500 = 1.39
ABA2	1500	2.77(3)	12.4/4.77/34/4.77/12.4	3840 (1170–1500–1170)	6270/4690 = 1.34

diffusive light scattering technique with high sensitivity. A light beam from the AlGaAs source (654 nm), with a typical spectral half-width of 18 nm, is focused on the measuring sample. Directly above the sample is an optical system that monitors the scattered intensity signal (*S*) of the sample while it is exposed to prescribed temperature alterations.[27–29] The relation between the calculated turbidity (τ) from the spectrophotometer experiments and the signal (*S*) from the cloud point analyzer is given by[27] $\tau\left(\mathrm{cm}^{-1}\right)=9.0\times10^{-9}\,S^{3.75}$.

For the measurements, 0.15 mL of the test solution is applied by a micropipette onto a specially designed glass plate. The plate is coated with a thin metallic layer functioning as a high reflectivity mirror. The sample surface is covered with highly transparent silicon oil in order to avoid evaporation of solvent at higher temperatures. A platinum resistance thermometer probes the temperature of the sample, and a compact thermoelectric device (array of Peltier elements) located close to the test solution is utilized to cool down and warm up the sample over a wide range of temperatures (–60 to +60 °C). In this work, the heating rate was set to 0.2 °C min^{-1}, and no effect of the heating rate on the signal was observed at low heating rates. All data from the cloud point analyzer will in this work be reported in terms of turbidity.

2.4. Phase Diagram Determination

The phase diagrams for aqueous solutions of the PLGA-PEG-PLGA block copolymers were determined by the tube inverting method.[30] Aqueous solutions of the copolymers were prepared at various concentrations. From each solution 2 mL was transferred to glass tubes. The tubes were sealed and kept in the water bath and heated up from 4 to 50 °C. The sol-to-gel transition temperature was determined by a flow or no-flow criterion over 30 s. The temperature was controlled at a heating rate of 0.2 °C min^{-1}, and the transition temperature was monitored at an accuracy of better that ± 1 °C. The results were reproducible within this accuracy.

2.5. Rheological Measurements

Oscillatory shear experiments were performed in an Anton Paar-Physica MCR 301 rheometer using a cone-and-plate geometry, with a diameter of 75 mm and a cone angle of 1°. The measuring apparatus is equipped with a temperature unit (Peltier plate), which provides an effective temperature control (±0.05 °C) for an extended time over the studied temperature range. The free surface of solutions was covered with a thin layer of low-viscosity silicone oil to prevent the dehydration of the samples at elevated temperatures. The observed viscosity value is practically unaffected by the oil layer. All measurements were performed at a heating rate of 1 K min^{-1}. Before the rheological measurements, the strain amplitude was checked to ensure that the measurements are conducted within the linear viscoelastic regime so that the dynamic storage modulus (*G′*) and loss modulus (*G″*) are independent of the strain amplitude.

2.6. SANS

The SANS-instrument at the JEEP-II reactor of IFE at Kjeller, Norway, was employed for the small angle neutron scattering measurements. The wavelength was set with the aid of a velocity selector (Dornier), using a wavelength resolution ($\Delta\lambda/\lambda$) of 20%. The neutron detector was a 128 × 128 pixel, ^{3}He-filled RISØ type, mounted on rails inside an evacuated detector chamber. The investigated scattering vector *q*-range was $8\times10^{-3}\le q\le0.3$ Å^{-1}. In all the SANS measurements, deuterium oxide (D_2O) was used as a solvent instead of H_2O in order to obtain good contrast and low background for the neutron-scattering experiments. The samples were introduced into 2 mm Hellma quartz cuvettes. To ensure good thermal contact, the measuring cells were placed onto a copper-base and mounted onto the temperature-controlled sample stage. The detector chamber was evacuated to reduce the scattering caused from air. Standard reductions of the scattering data, including transmission corrections, were done by including data collected from empty cell, beam without cell, and blocked-beam background. The data were converted to an absolute scale (coherent differential cross section ($d\Sigma/d\Omega$)) via normalization based on direct beam measurements.

Model fittings of the scattering data were made (on an absolute scale) taking into account the molecular parameters of the system (see description of the models below). The calculated scattering length densities (ρ) for neutrons for PEG and PLGA are 0.64×10^{10} cm^{-2}[31] and 1.60×10^{10} cm^{-2},[32] respectively. Since the solvent D_2O has a value of $\rho=6.3\times10^{10}$ cm^{-2}, both PEG and PLGA therefore gives good intrinsic contrast. However, if the PEG block is highly solvated (corona), the contribution from PEG will be reduced. Since the mass densities of PEG (ρ_m = 1.13 g cm^{-3}) and PLGA (ρ_m = 1.2 g cm^{-3}) are close to that of D_2O (1.11 g cm^{-3}), the volume concentration that is relevant for SANS, will be close to the weight percentages used in this work.

3. Results and Discussion

3.1. Turbidity

For block copolymers with temperature responsive blocks, turbidity is a valuable tool to monitor thermodynamic changes and aggregation with temperature. A rise in turbidity may indicate growth of hydrophobic associations

among the micelles or self-assemblies of chains. The temperature dependencies of the turbidity at different concentrations for the two triblock copolymers with different length of the PEG-spacer are depicted in Figure 4. The temperature at which the turbidity rises from the baseline is considered as the cloud point (CP). The results indicate that the PLGA blocks are sensitive to temperature and this is illustrated by the abrupt rise of the turbidity in Figure 4a. This suggests that the sticking probability increases strongly with increasing temperature above the CP, and intermicellar aggregates are formed. For the dilute solutions (1 wt%), the value of CP is ≈27 °C for $PLGA_{1170}$-PEG_{1000}-$PLGA_{1170}$ and 37.5 °C for $PLGA_{1170}$-PEG_{1500}-$PLGA_{1170}$ copolymer with the longer PEG spacer. A longer PEG block makes the copolymer more hydrophilic and a higher temperature is required to trigger the growth of association complexes. For semidilute (20 wt%) solutions, the CP is 21 and 43 °C for $PLGA_{1170}$-PEG_{1000}-$PLGA_{1170}$ and $PLGA_{1170}$-PEG_{1500}-$PLGA_{1170}$ samples, respectively. As expected, the value of CP is higher, both at the low and high polymer concentration for the copolymer with the long PEG spacer as a result of amended hydrophilicity. For the copolymer with the short PEG spacer, increased polymer concentration favor a lower CP value (27 → 21 °C). The drop in cloud point with increasing polymer concentration seems to be a general feature for many thermoresponsive copolymers and homopolymers.[5,27,28,33,34] The turbidity and cloud point behavior may be rationalized in the following scenario. As the temperature rises the moieties become gradually more "sticky" and higher concentration favors higher collision frequency of the species and this leads to larger association complexes and enhanced turbidity. The impacts of concentration and temperature on the formation of aggregates in polymer solutions have been addressed in several theoretical approaches.[35–38]

In contrast, the cloud point for the copolymer with the long spacer increases (37.5 → 43 °C) with increasing polymer concentration. The hypothesis for this behavior of the $PLGA_{1170}$-PEG_{1500}-$PLGA_{1170}$ copolymer is that at a high concentration of the copolymer, the long spacer chains generate bridging of micelles, and a network of interpenetrating and bridged chains is evolved. The conjecture is that at this concentration the network becomes fairly homogeneous with hydrophobic microdomains evenly distributed in the network and this leads to a higher CP than for dilute solution where the aggregates are not yet organized. In this context, it is interesting to note a previous study[34] on a temperature sensitive linear ABCBA pentablock tercopolymer with different length of the PEG spacer. It was found that a longer PEG block favored the formation of virtually transparent gels at elevated temperatures.

Figure 4b shows the turbidity data over an extended temperature range for dilute solutions (1 wt%) of the two copolymers. It is interesting to note that at high temperatures, an abrupt decrease in the turbidity is observed for

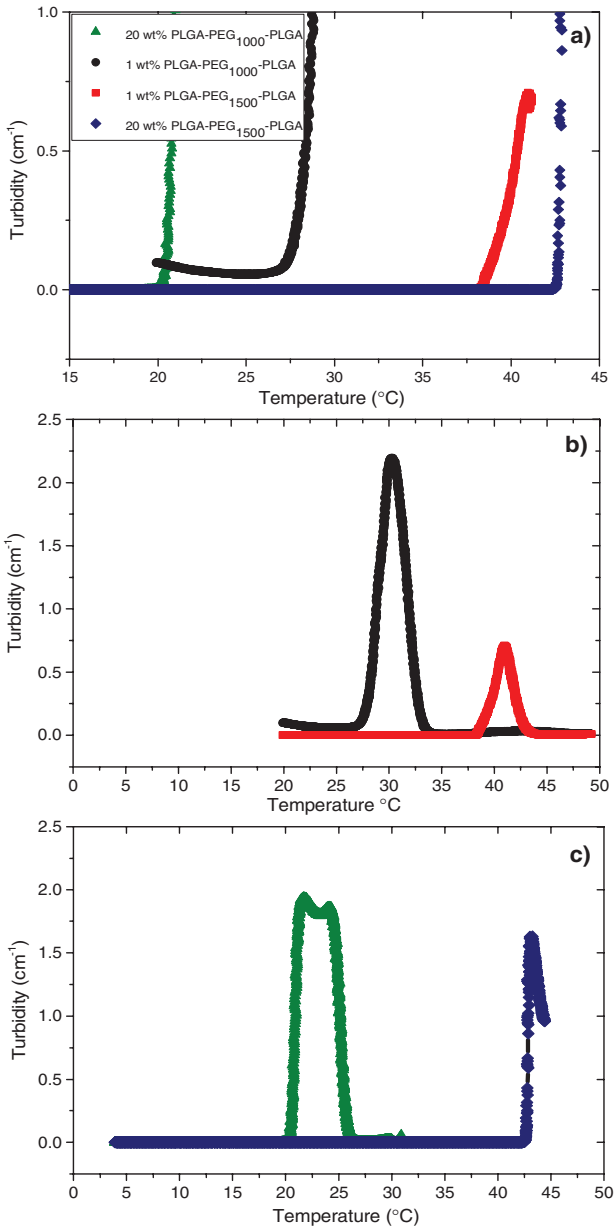

Figure 4. a) Overview of the determination of cloud points for 1 and 20 wt% aqueous samples of $PLGA_{1170}$-PEG_{1000}-$PLGA_{1170}$ and $PLGA_{1170}$-PEG_{1500}-$PLGA_{1170}$. The whole temperature profiles of the turbidity for b) dilute (1 wt%) and c) semidilute (20 wt%) systems of the two copolymers.

both copolymers, but the amplitude of the transition peak is more pronounced for the copolymer with a short PEG spacer. The reason for this is probably that larger hydrophobic microdomains are formed for the more hydrophobic polymer. As will be discussed below in detail in connection with the analysis of the viscosity results, the peak feature is ascribed to the evolution of intermicellar structures up to the maximum of the peak, followed by contraction and disintegration of clusters at higher temperatures. Temperature dependencies of the turbidity for

semidilute solutions (20 wt%) of the two copolymers are depicted in Figure 4c. The profile of the turbidity curves is reminiscent of those for dilute solutions. As demonstrated below from the rheology results, the turbidity maximum is located in the gel region, and at higher temperatures where the turbidity drops quickly our hypothesis is that the gel-network is disrupted as a consequence of compaction of the hydrophobic microdomains and a structural reorganization from connected micelles in the gel region to packed cylinders at higher temperatures (cf. the discussion of the SANS results). The drop in turbidity at high temperatures is less marked for the copolymer with the long spacer; thus indicating less fragmentation of the gel-network. This can probably be ascribed to the ability of this copolymers to from bridges between the micelles at elevated temperatures and thereby improve the connectivity.

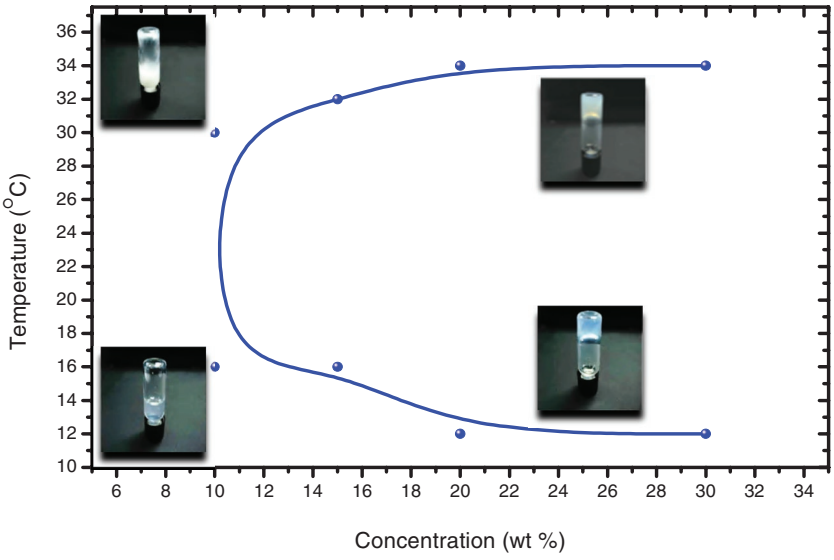

Figure 5. Illustration of a temperature–concentration phase diagram of aqueous solutions of the $PLGA_{1170}$-PEG_{1000}-$PLGA_{1170}$ triblock copolymer.

In previous studies on PEO-PLGA-PEO triblock copolymers it was reported[39,40] that the turbidity behavior depends only on the temperature but not on the copolymer concentration. The differences in turbidity and cloud point behavior can probably be related to the PEG/PLGA or PEO/PLGA ratio, which governs the overall hydrophobicity of the copolymer and the sticking probability of the moieties. In addition, the molecular architecture of the triblock copolymer may influence the behavior significantly.

3.2. Phase Diagram and Rheology

The phase diagram for $PLGA_{1170}$-PEG_{1000}-$PLGA_{1170}$ triblock copolymer in aqueous solution is depicted in Figure 5. At low temperatures, the system forms a free-flowing liquid at all the studied concentrations. In the semidilute and concentrated concentration regime (10–30 wt%), the solutions undergo a reversible sol-to-gel transition as the temperature is increased. As showed by the inset images in the gel region, the gel becomes more turbid with increasing temperature. At a polymer concentration of about 20 wt%, the gel region is rather broad, from ≈12 to 33 °C. At still higher temperatures a macroscopic phase separation takes place. In the dilute concentration regime, no gel is formed and the solution transforms to a turbid suspension of large aggregates.

The process of gelation may be rationalized in the following way. To form a gel network it is necessary to establish a delicate balance between network connectivity and swelling.[41] If the connectivity provided through the hydrophobic microdomains is too dominating, macroscopic phase separation takes place. If, on the other hand, the swelling power is dictating and the physical crosslinking zones are in deficiency, a gel-network is not formed. For the PLGA-PEG-PLGA triblock copolymer, the network in the semidilute concentration range is created through packing and bridging of micelles to various intermicellar structures (these structures will be discussed in detail when the SANS results are presented); the status of this network (transient or gel network) will depend on the ratio of hydrophilic groups (PEG) and hydrophobic (PLGA) groups and the temperature. The growth of hydrophobic junction zones at higher temperatures generates connectivity of the network and a gel is formed; at sufficiently high temperatures the gel becomes turbid and eventually we have a "white gel".[42] The swelling effect is provided by the PEG block, but at higher temperatures this effect is weakened because PEG has a lower critical solution temperature at temperatures around 100 °C. In this context, it is interesting to note that in a number of theoretical studies on temperature-responsive gels, the interference between gelation and two-phase separation was recognized.[43–46] These investigations revealed that thermoreversible gelation is accompanied by a feature of phase separation. In view of this, the influence of temperature on the turbidity was monitored as discussed above; the results support the close relationship between gelation and incipient phase separation. Actually, it has been argued that there is an interference between reversibly gelling polymer systems and macroscopic two-phase separation.[44]

Oscillatory sweep experiments were used to investigate the viscoelastic properties of dilute and semidilute samples of $PLGA_{1170}$-PEG_{1000}-$PLGA_{1170}$ and $PLGA_{1170}$-PEG_{1500}-$PLGA_{1170}$

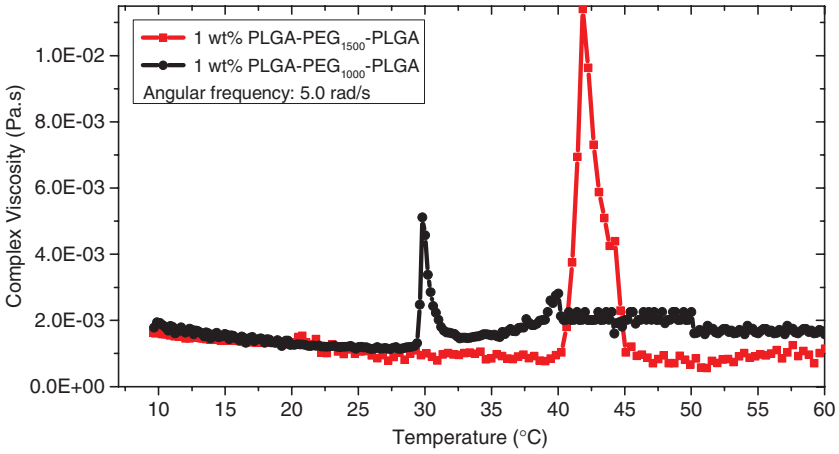

Figure 6. Temperature dependencies of the complex viscosity for the copolymers indicated at a polymer concentration of 1 wt% and an angular frequency of 5.0 rad s^{-1}.

and to determine the gelation temperatures of the two copolymers in semidilute solutions. Figure 6 shows the influence of temperature on the complex viscosity for the two copolymers in the dilute concentration regime at a concentration of 1 wt%. There is some noise in the data because of the low viscosity, but a peak is clearly observed for each polymer. As expected, the peak is shifted to a higher temperature when the PEG-spacer length is increased since the polymer becomes more hydrophilic. A close inspection of the curves reveals a moderate decrease of the complex viscosity (η^*) up to approximately the cloud point. This suggests that the moieties are initially slightly compressed upon a temperature raise. This type of behavior has been reported for PLGA-PEG-PLGA copolymers.[47–50] After passing CP, η^* rises with increasing temperature and this is attributed to loose intermicellar structures or aggregates; this conjecture is supported by the turbidity results discussed above. This can probably be ascribed to enhanced sticking probability of the species at temperatures above CP and the formation of loose interchain structures, where the driving force is dehydration and hydrophobic interactions.[51–54] As the temperature rises, η^* passes through a maximum and falls off rapidly as the temperature increases. The agglomerates consist of a number of interconnected micelles and as the temperature rises the cluster and the micelle components will contract and this process may gradually lead to a breakup of the aggregates because of the contraction of the subunits and perhaps also structural changes of the sub-structures as the SANS experiments seem to suggest. There are several studies[51–54] on aqueous solutions of thermoresponsive amphiphilic copolymers, where similar features have been reported, i.e., the formation of large aggregates with a loose structure at elevated temperatures, followed by a tremendous size reduction at very high temperature. These findings were interpreted in terms of the formation of large aggregates, followed by dissociation of the clusters to micelles at high temperature due to dehydration.

An interesting issue to discuss in this context is how the compressed sub-structures will interact with each other. Based on both theoretical and experimental studies[55–57] on systems approaching phase separation, it has been argued that the sticking probability may be significantly reduced for very compact structures. This may elucidate why the contracted moieties do not associate again at the highest considered temperatures, as shown by the viscosity data in Figure 6.

Now the oscillatory shear viscosity results for the copolymers in the semidilute concentration regime will be presented and discussed. Temperature dependence of the complex viscosity for a semidilute sample of the $PLGA_{1170}$-PEG_{1000}-$PLGA_{1170}$ triblock copolymer is displayed in Figure 7a. The contour of the viscosity curve is similar to that observed for the dilute solution, but the origin is different. In this case we are in the semidilute concentration regime, and the micelles form a transient network at low temperatures. As the temperature rises the hydrophobic microdomains grow and the connectivity is established and the gel-network is evolved at about 15 °C (cf. the discussion below). At higher temperatures, the drop of the viscosity suggests that the gel-network breakup and at sufficiently high temperatures the viscosity assumes values comparable with those at low temperatures. As argued in connection with the discussion of the turbidity results, our hypothesis is that due to the compression of the hydrophobic junction zones and structural reorganization, the connectivity in the gel-network is gradually lost as the temperature increases.

According to the method of Winter and Chambon,[58] the gelation temperature can be determined by observation of a frequency-independent value of tan δ ($=G''/G'$) obtained from a multi-frequency plot of tan δ versus temperature. Here G' and G'' are the dynamic storage and loss modulus, respectively. Alternatively, the gelation temperature can also be obtained[59] by plotting the "apparent" viscoelastic exponents n' and n'' ($G' \approx \omega^{n'}$, $G'' \approx \omega^{n''}$) calculated from the frequency dependence of G' and G'' at different temperature and observing a crossover where $n' = n'' = n$ (see the inset graph b) in Figure 7).

Figure 7 shows a decrease in the damping factor during the gel formation of the $PLGA_{1170}$-PEG_{1000}-$PLGA_{1170}$ copolymer solution and this trend indicates enhanced elasticity of the thermogelling network with raising temperature. Both methods yield virtually the same gelation temperature (15 °C). At the gel point temperature, the G' and G'' curves become parallel and power laws in frequency (see inset

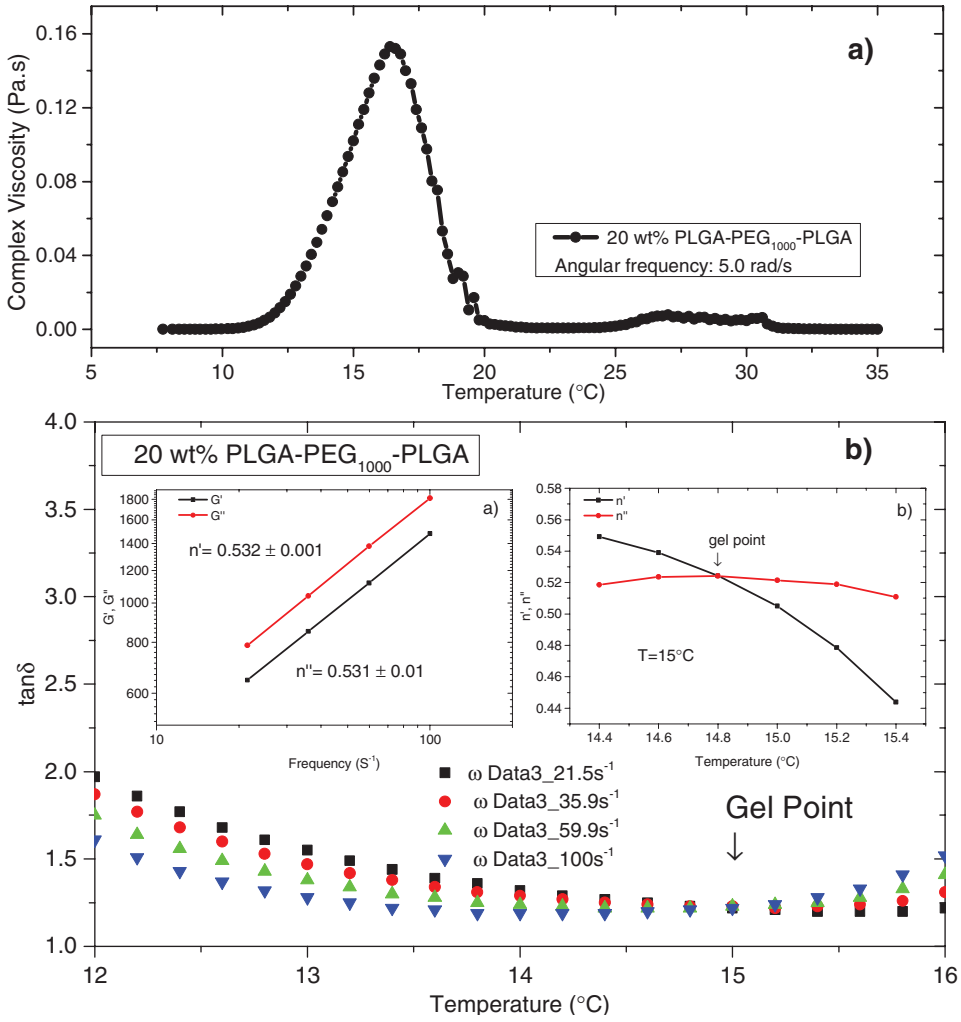

Figure 7. a) Temperature dependence of the complex viscosity at an angular frequency of 5 rad s^{-1} for the copolymer and concentration indicated. b) Illustration of methods for the determination of the gel point. Viscoelastic loss tangent (tan δ) as a function of temperature for the system and frequencies indicated. The upper inset plot to the right depicts changes of the apparent exponents n' for the storage and n'' for the loss moduli during the course of gelation. The upper inset plot to the left shows the power law behavior of the dynamic moduli at the gel point temperature.

b) in Figure 7b) as predicted by the Winter and Chambon model.[58] The gel temperature for the copolymer with a longer PEG spacer was found in the same way to be 46 °C. Since this copolymer is more hydrophilic, a higher temperature is required to create the hydrophobic junction zones necessary to establish the connectivity of the gel network.

In this study, the theoretical model of Winter and Chambon is utilized to describe the gel strength for an incipient gel, according to the following relationship[58]

$$G' = \frac{G''}{\tan\delta} = S\omega^n \Gamma(1-n)\cos\delta \quad (1)$$

where $\Gamma(1-n)$ is the gamma function, n is the relaxation exponent, δ is phase angle between stress and strain, and S is the gel strength parameter.

Muthukumar elaborated a theoretical model,[60] based on the assumption that variations in the strand length between cross-linking points of the incipient gel network give rise to changes of the excluded volume interactions, to rationalize values of n in the whole physically accessible range ($0 < n < 1$). In this approach, a relationship between n and the fractal morphology of the incipient gel network was established through the following expression

$$n = \frac{d(d+2-2d_f)}{2(d+2-d_f)} \quad (2)$$

where d ($d = 3$) is the spatial dimension and d_f is the fractal dimension, which relates the mass of a molecular cluster to its radius of gyration by $R^{d_f} \approx M$. Larger values of d_f suggest a more compact network structure.

The values of the parameters for $PLGA_{1170}$-PEG_{1000}-$PLGA_{1170}$ are $n = 0.53$, $d_f = 2.0$, and $S = 16$ PaS^n, while for the copolymer with the longer PEG-spacer $n = 0.9_8$, $d_f = 1.3$, and $S = 0.2$ PaS^n. The values of the fractal dimension

suggest that the incipient gel network is more open for the copolymer with the long PEG-spacer. This is attributed to the higher flexibility of the polymer chains with the long PEG-spacer and bridges may be formed between micelles. We note that the gel strength is significantly higher for the copolymer with short PEG-spacer and we recall that S is sensitive to changes of the strand length between the junction zones in the gel network and the strength of the hydrophobic couplings. Due to the higher flexibility and less hydrophobicity of $PLGA_{1170}$-PEG_{1500}-$PLGA_{1170}$ copolymer, we anticipate a longer average strand length and less hydrophobic interactions and therefore a lower value of S for this copolymer.

3.3. Small Angle Neutron Scattering

To gain insight into the micellar structure on a mesoscopic dimensional scale, SANS experiments were performed on dilute (1 wt%) and semidilute (20 wt%) samples of the two copolymers at various temperatures. Before the results are presented and discussed, a brief summary is given of the models used in the analyses of the SANS results.

The SANS patterns were fitted to different model structures as described in the text. The core–shell spherical model has a form factor $P(q)$ described by

$$P(q)=\frac{\text{scale}}{V_s}\left[\frac{3V_s(\rho_c-\rho_s)j_1(qR_c)}{qR_c}+\frac{3V_s(\rho_s-\rho_{solv})j_1(qR_s)}{qR_s}\right]^2 \quad (3)$$

where V_s is the particle volume including the outer shell, V_c is the volume of the core, R_s is the radius of the shell, and R_c is the radius of the core, thus $R_s = R_c + d$, where d is the thickness of the shell. The parameter ρ_c is the scattering length density of the core, ρ_s is the scattering length density of the shell, and ρ_{solv} is the scattering length density of the solvent. $j_1(x) = (\sin x - x \cos x)/x^2$, and scale is a scale factor proportional to the sample concentration.

The core–shell cylinder model, that was also employed in this study, has a form factor $P(q)$ described by

$$P(q)=\frac{\text{scale}}{V_s}\int_0^{\frac{\pi}{2}} f^2(q,\alpha)\sin\alpha\, d\alpha \quad (4)$$

where it has been assumed an overall random orientation of cylinders, and where

$$f(q,\alpha)=2(\rho_c-\rho_s)V_c j_o(qH\cos\alpha)\frac{J_1(qR_c,\sin\alpha)}{qR_c\sin\alpha} +2(\rho_s-\rho_{solv})V_s j_o\left[q(H+t)\cos\alpha\right]\frac{J_1(qR_s\sin\alpha)}{qR_s\sin\alpha} \quad (4a)$$

where α is the angle between the axis of the cylinder and the q-vector. V_c is the volume of the cylindrical core, V_s is the total cylinder volume (including the shell), thus $V_c = \pi R_c^2 L$ and $V_s = \pi R_s^2 L$, where L is the length of the core, R_c is the radius of the core, and t is the thickness of the shell ($R_s = R_c + t$). The total length of the outer shell is given by $L + 2t$. The parameters ρ_c, ρ_s, and ρ_{solv} are the scattering lengths as defined earlier. J_1 is the first order Bessel function, and $j_0(x) = \sin x/x$.

As mentioned in the experimental section, the scattering length densities employed in this study are 0.64×10^{10} cm^{-2} for PEG[31] and 1.6×10^{10} cm^{-2} for PLGA.[32] The model fitting was implemented via the NIST analysis package,[61] and the models are described in more detail in ref.[62].

The ellipsoidal model that was also used in one case has a form factor similar to that of the cylinder model, and is not listed here. However, details can be found in ref.[62] For the case (i.e., the 20 wt% systems) where interaction between the particles had to be taken into account, non-Coulombic hard sphere interaction (excluded volume effects) model was employed.

Let us first discuss the SANS results for dilute solutions of the two amphiphilic triblock copolymers. Figure 8 shows the SANS intensity profiles for 1 wt% solutions of $PLGA_{1170}$-PEG_{1000}-$PLGA_{1170}$ and $PLGA_{1170}$-PEG_{1500}-$PLGA_{1170}$ at different temperatures. The data points have been fitted with the aid of different models as discussed above.

The scattered intensity data for the copolymer with the short PEG-spacer exhibits an intricate behavior at the different temperatures considered and some comments are needed. At 10 °C, the data is fitted by employing a prolate ellipsoid model, giving a minor axis (including shell) of R_{min} = 72 Å and a major axis of about R_{maj} = 220 Å, which yields an axial ratio of ≈3. It should be mentioned that it was not possible to acquire reasonable fit to this data employing a spherical model. Actually, even if different degrees of polydispersity effects were taken into account a spherical model could not be utilized to obtain a rational fit (S1, Supporting Information). At 20 °C, the best fit to the SANS data was achieved using a disk-like micelle or oblate ellipsoid model, yielding a minor axis (including shell) to be ≈60 Å, and the major axis is very large ≈500 Å, giving an axial ratio of ≈8, which suggests an extended object. However, both prolate and cylindrical models gave poor fits (cf. Figure 9) and cannot portray the data for the copolymer with a short spacer. In addition, the SANS data at 20 °C and at low q-values shows a slope close to −2, which is an indication of disk-like objects. The drop of the scattered intensity at higher temperatures (30 °C and above) announces incipient phase separation and sedimentation of polymer out of the neutron beam.

In the case of the copolymer with a long PEG-spacer (Figure 8, panel to the right), the effect of temperature is modest. At all temperatures, the scattered intensity data can be fitted by a spherical core–shell model and the results are displayed in the inset table. There is no

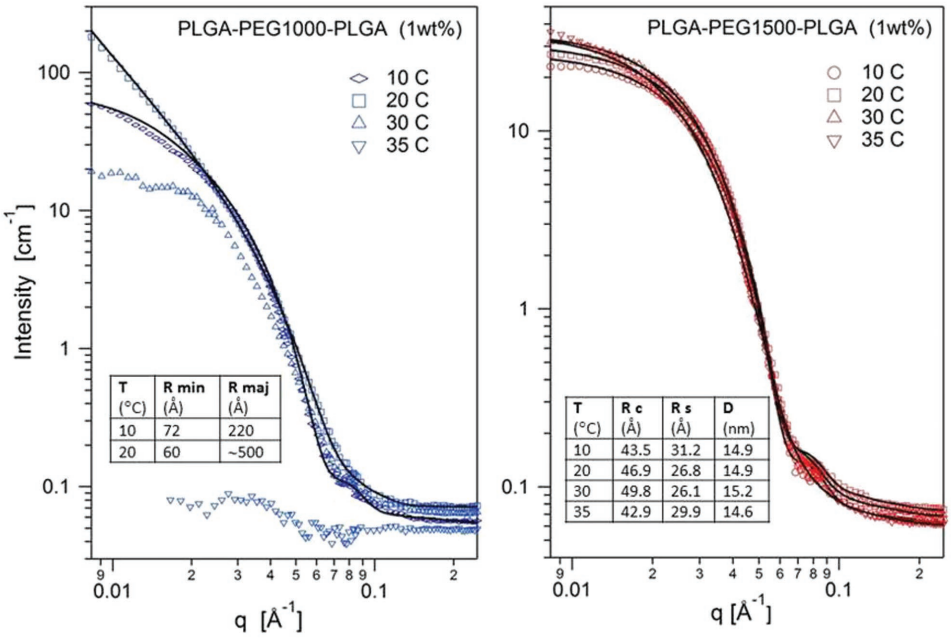

Figure 8. SANS intensity profiles plotted versus the scattering vector q for 1 wt% solutions of PLGA-PEG$_{1000}$-PLGA and PLGA-PEG$_{1500}$-PLGA at the temperatures indicated. The inset table shows the values of the parameters from modeling. For PLGA-PEG$_{1500}$-PLGA a core–shell model was used, with R_c being the core radius and d the shell thickness (D is the diameter). For PLGA-PEG$_{1000}$-PLGA different asymmetric models were used, with R_{min} and R_{maj} being the minor and major axis, respectively, as explained in the text.

significant temperature effect, but it seems that rising temperature leads to minor increase of the R_c and a small decrease of the shell thickness (d), while the diameter of the whole micelle is practically constant and independent of temperature. In this temperature interval, we do not expect any major temperature changes because the temperatures are well below the cloud point.

In Figure 9, the prominent features of the copolymers in dilute solutions are summarized. Note that all plots have been made with the same y-scale in order to compare also the absolute scattering values. It is clearly seen that the PLGA-PEG$_{1000}$-PLGA copolymer shows higher scattered intensity levels at low q than PLGA-PEG$_{1500}$-PLGA as a result of the asymmetric structures for the polymer with a short PEG-spacer. The polymer with a short PEG-spacer, the scattered intensity data can be well portrayed by the prolate ellipsoid model at 10 °C, whereas at 20 °C the SANS data are well-described by an oblate ellipsoid model. Since the axial ratio is high (about 8) in the latter case, we were lead to believe that a cylinder

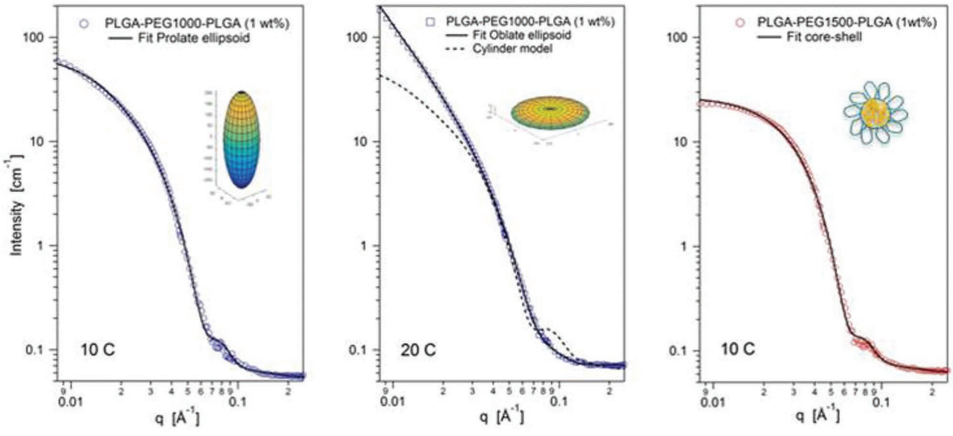

Figure 9. SANS intensity profile and fit (solid line) plotted versus the scattering vector q for 1 wt% solutions of PLGA-PEG$_{1000}$-PLGA at 10 °C (left) and 20 °C (middle), and PLGA-PEG$_{1500}$-PLGA at 10 °C (right). For PLGA-PEG$_{1000}$-PLGA the fit is to a prolate ellipsoid at 10 °C, and to an oblate ellipsoid 20 °C with also the curve for a cylindrical model shown as a dashed line. For PLGA-PEG$_{1500}$-PLGA the fitted curve is a spherical core–shell model. Note that all plots have been made with the same y-scale in order to compare also the absolute scattering values.

model may also be an adequate model, but as is observed from the dashed line in the middle panel this does not result in a reasonable fit. Illustration of the prolate and oblate objects is depicted in the insets in Figure 9. When it comes to the asymmetric scattering models we have employed in the fitting of the SANS data, especially the oblate model, we can only state that our fitting models portray the data very well. However, we cannot exclude other types of structures because at some temperature conditions it is possible that the degree of polydispersity is very high so the system is in a transient condition where the scattering pattern is strongly modified. The panel to the right shows that the scattered intensity can be well described by a spherical core–shell structure for the copolymer with a long PEG-spacer. The fundamental differences in behavior between dilute solutions of PLGA-PEG_{1000}-PLGA and PLGA-PEG_{1500}-PLGA can probably be traced to the more hydrophilic character and higher flexibility of the copolymer with a longer PEG-spacer.

In this section, the SANS properties of semidilute solutions of these two copolymers will be discussed and analyzed. As for the dilute solutions of these copolymers, some novel and special structural features of these semidilute systems will be disclosed.

Figure 10 shows scattering profiles for a semidilute sample of PLGA-PEG_{1000}-PLGA at different temperatures, covering both sol and gel states. At a low temperature (10 °C), the solution is considered to consist of micelles with a PLGA core and PEG-corona; possibly at this high concentration micelles will be interconnected by sharing PLGA chains, but this situation will depend on the length of the PEG-chain. In any case, the system resembles a population of quasi-separate micelles with some average interaction distance. The distinct peak or correlation peak (located at $q = 0.03$ Å^{-1}) at this low temperature suggests that there is a significant interaction between the micelles, i.e., the micelles feel strongly the presence of their neighbors and the intermicellar distance is d_{int} = 21 nm ($d_{int} = 2\pi/0.03$). At this low temperature, the hydrophobic effect of the PLGA block is not pronounced and each micelle contains chains that extend far out from the micellar surface. By fitting the data to the spherical core–shell model with a non-Coulombic hard sphere interaction (excluded volume effects), the radii of the core and thickness of the corona are R_c = 6.5 nm and d = 3.2 nm, respectively (D = 19.4 nm). A core radius of 6.5 nm is shorter than that of a fully extended (trans) PLGA chain. The latter can be roughly estimated to about 10 nm, based on a 1170 Da PLGA block and assuming one PLGA segment having a mole mass of 94 Da and extension of 8 Å (six bonds). Thus the PLGA chain adopts a somewhat collapsed configuration in the core. This is consistent with the finding by Riley et al.[31] in their work on PLA-PEG systems.

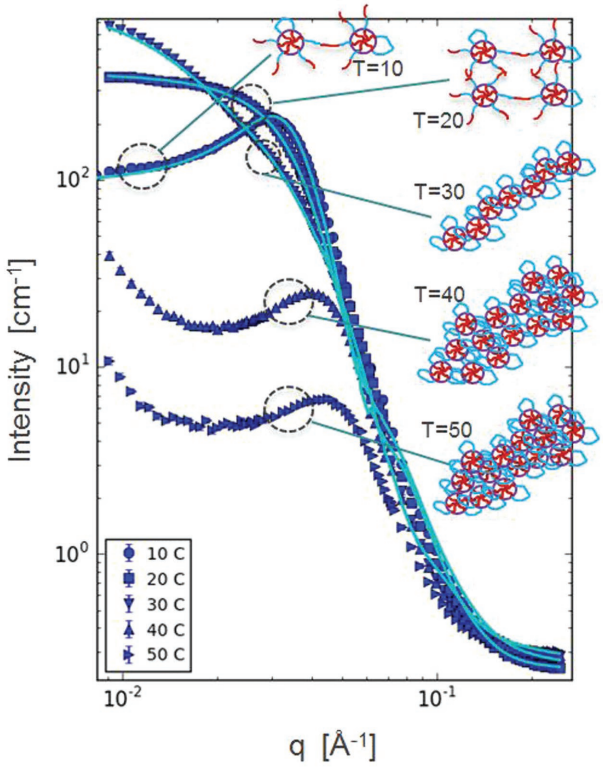

Figure 10. SANS scattered intensity profiles for 20 wt% solutions of PLGA-PEG_{1000}-PLGA at the temperatures indicated. The continuous lines in the figure represent fits of the data at temperatures of 10, 20 and 30 °C data.

As discussed above, a sol-to-gel transition takes place at higher temperatures and at 20 °C a gel is formed. It is interesting to note that at this temperature the correlation peak vanishes. This is an intriguing feature that probably can be attributed to a loss of the previously well-defined distance between the micelles as they create a gel-like network. This finding suggests that the network of interconnected micelles is organized in a quite irregular manner, i.e., loss of the organized 3D-structure that produced the well-defined correlation peak. There are very few small angle scattering studies on PLGA-PEG-PLGA systems, but it has been argued that the gel network is irregular. Yu et al.[63] suggested that micelles are formed and they are further percolated to form a gel with a macroscopically inhomogeneous micelle network. In a work by Zhang et al.[64] it was stated that the physical gelation is associated with a random fractal, instead of a regularly ordered packing of micelles. Quite recently it was argued that a thermogel was formed with a percolated micelle network. The fitting yields a core radius of R_c = 6.2 nm and d = 2.8 nm, or a micellar diameter of 18 nm. This suggests that the overall size of the micelles has only slightly been reduced in connection with the disappearance of the correlation peak.

At 30 °C, a different shape of the scattered intensity profile emerges compared with the other temperatures. At intermediate q values the scattered intensity curve assumes a profile (slope: –1) that is characteristic of thick rod-like entities. Thus it is rational to apply a cylindrical model to gain information about this system at this temperature. The modeling gives a cylinder length of 34.3 nm and a radius of 5.6 nm. If the shell of 2.6 nm is included, this yields a cylinder diameter of 16.4 nm. This diameter is rather small, of the order found for the micelles at lower temperatures and this may indicate that the micelles are ordered along a line as reported previously.[63] We may note that the core diameter of the cylinder is 11.2 nm, which is smaller than was found for the micelles at 10 and 20 °C. This may suggest that the core is contracted due to increased hydrophobicity at elevated temperatures. The fact that no correlation peak is visible at this stage indicates that there is no well-defined mesh size in the network, but probably an irregular network. In view of the rheological and turbidity results it is likely that no percolated network is formed, but rather many of the cylinders are free to move or are linked at only one end and only a transient network is formed. This is actually consistent with the viscosity results discussed above.

At 40 °C, a new correlation peak emerges that is centered at 0.04 Å^{-1} (d_{int} = 2π/0.04 = 15.7 nm) and this average correlation distance is of the order of the size of a micelle, and can only arise when micelles are in close contact. This advocates formation of thick "cylinders", consisting of several micelles packed side-by-side. The value d = 15.7 nm is somewhat smaller than observed at lower temperatures, e.g., 18 nm at 20 °C. This demonstrates clearly that the micelles pack tightly in this configuration. The question is whether these moieties are packed in an ordered hexagonal packing or a more irregular packing. In a previous SANS study[65] on surfactant-based rigid gel mesophase, hexagonal and lamellar microstructures were detected and the scattered intensity profiles of these systems were characterized by the appearance of a secondary peak at higher q values. In a SAXS investigation[66] on the phase behavior of a symmetric styrene-isoprene diblock copolymer in a styrene-selective solvent, coexistence of both body-centered cubic and hexagonally close-packed sphere phases acted at higher concentrations. The characteristic feature of these phases was the appearance of secondary peaks, whereas for disordered phases no secondary peak was observed. In the light of this and the fact that we have not observed a secondary peak, the conjecture is that the packing of the cylinders is probably not very ordered. It is interesting to note that at this temperature, a strong upturn in the scattered intensity is observed at low q values. This signalizes that large structures are evolved, and is a fingerprint of the thickness of the "rod" formed by the micelles. There is no sign of a plateau region (therefore fitting was not intended at this temperature), and it can be argued that the rods are in principle thicker than the lower value probed here, that is, 2π/0.009 Å^{-1}, or 70 nm. This shows that on average a large number of micelles form the clusters laterally when forming this thick rod.

At 50 °C, the scattered intensity profile of the sample is similar as observed at 40 °C, but with a lowering of the overall signal as a result of material loss (sedimentation as a result of macroscopic phase separation) in the path of the neutron beam. The packing distance at this temperature is 2π/0.05 Å^{-1} = 12.5 nm. This illustrates that the hydrophobic effect has generated even a further compression of the rods, while keeping the number of micelles in each "rod" practically the same. The low q-behavior is quantitatively the same as at 40 °C.

To gain insight into the fractal dimension of a system, the SANS profile of the sample is frequently analyzed in the high q range. Figure S2 (Supporting Information) illustrates the scattered intensity profile (the background scattering has been subtracted) for the PLGA-PEG$_{1000}$-PLGA copolymer at a concentration of 20 wt%. At high q-values in a log-log plot we observe a well-defined slope of –4. In the interpretation of this behavior, it should be remembered that at these high q-values small local substructures (sizes of the order of 1 nm) inside the micelle are probed, and not the network coupling zones that are addressed in the Muthukumar model[60] (above a value of the fractal dimension of 2 was reported for this system). The SANS scattered intensity essentially records the contribution from the core inside the micelle (much larger contrast than from the corona); this result suggests that the core of PLGA is compact for the system at the considered temperatures. A slope of –4 at high q, theoretically predicts that the surface of the core is smooth. The picture that emerges from the SANS results is that the cores of the individual micelles are virtually intact as the gel-network is evolved, but they are organized in a manner so that the connectivity in the network is established. The value of the fractal dimension of 2 we observed above from the Muthukumar approach is not far away from the value of 2.5 obtained from percolation statistics.[67]

It is well recognized in the literature[39,48,63,64,68,69] that the block lengths of PLGA and PEG in copolymers of the type PLGA-PEG-PLGA will have a critical impact on the properties of the copolymers in solution. As demonstrated from the turbidity and rheology results above, a longer PEG-spacer will make the copolymer more hydrophilic and the cloud point and viscosity transition are shifted to higher temperatures.

To reveal the impact of PEG-spacer length on the SANS results, the scattered intensity profiles of the two block copolymers are compared in Figure 11. It is obvious that similar scattering profiles are observed for both

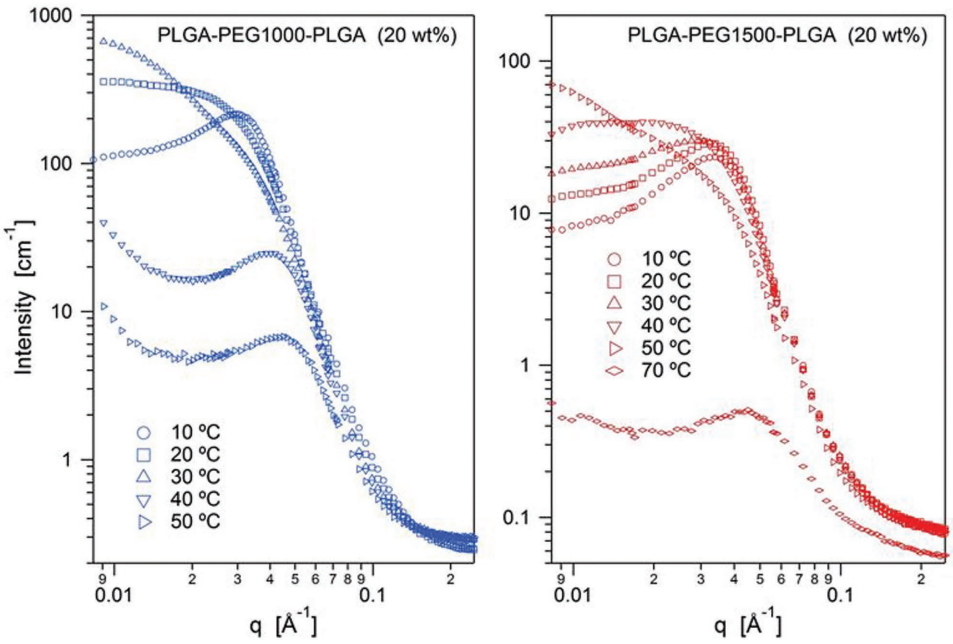

Figure 11. Small-angle neutron scattering for 20 wt% solutions of PLGA-PEG_{1000}-PLGA (left) and PLGA-PEG_{1500}-PLGA (right) at various temperatures.

copolymers, but characteristic features of the PLGA-PEG_{1000}-PLGA sample are shifted to a higher temperature for the PLGA-PEG_{1500}-PLGA sample. For instance, the gel profile (no correlation peak) is observed at 20 °C for the PLGA-PEG_{1000}-PLGA block copolymer, whereas for the PLGA-PEG_{1500}-PLGA sample this feature appears at 40 °C. The only significant difference in the scattered intensity of the copolymers is a generally lower intensity level for the polymer with the long PEG-spacer (see Figure 11). From the similar scattered intensity profiles observed for these two copolymers, it can be concluded that the two samples have the same general structures, but at different temperatures.

By using a spherical core–shell model to fit the SANS data for the copolymer with a longer PEG-spacer a micellar diameter of 18.2 nm is obtained at 10 °C, which is slightly smaller than that (D = 19.4 nm) for the copolymer with a short spacer. In addition, the maximum of the correlation peak at 10 °C is located at a slightly higher q-value of $\approx q = 0.034$ Å^{-1}, giving an average intermicellar distance of $2\pi/0.034 = 18.5$ nm (compared to 21 nm found for the copolymer with a short spacer). This is just above the diameter of one micelle, implying vigorous micellar interactions. This enlightens the fact that the correlation peak is even better defined in this case than for the copolymer with short spacer. The shorter average intermicellar distance for the PLGA-PEG_{1500}-PLGA copolymer suggests a larger number of entities per unit volume, and this is only possible if there are fewer chains inside each micelle in comparison to the micelles of the short spacer copolymer. This difference in behavior between the copolymers can be rationalized in the following way. In the samples with the long PEG-spacer, the surmise is that the flexibility of the spacer will allow the two PLGA blocks to occupy the same micellar core. However, this is a rather space consuming conformation, suggesting that only a relatively small number of chains can join together in this way, and thereby creating a "flower-like" micelle as suggested previously.[45]

For the copolymer with the short spacer, on the other hand, the PEG-spacer is too short to turn back on itself (this requires too much bending energy for the chain, which is entropically unfavorable) and thereby allowing the PLGA blocks to occupy the same micelle. As a result, most micelles formed with the short PEG-spacer copolymer have a micelle core with only one PLGA block from each chain. At low temperatures, the PLGA block for the PLGA-PEG_{1000}-PLGA copolymer will find it more energetically advantageous to protrude out in the solution. However, when the hydratization is reduced (increasing temperature) and the PLGA block is protruding out in the surrounding solvent, it can easily be accommodated into the core of a neighbor micelle as soon as the hydrophobicity of the PLGA blocks is sufficient. This mechanism may explain why the PLGA-PEG_{1000}-PLGA copolymer forms a gel at a much lower temperature than the PLGA-PEG_{1500}-PLGA system. When it comes to the copolymer with a longer PEG-spacer, where generally both its PLGA blocks are located in the same micelle, a more efficient stabilization of the micelles should occur at low temperatures where individual micelles exist. This is supported by the SANS results of PLGA-PEG_{1500}-PLGA copolymer, where

it can be seen that the scattered intensity profile is practically the same in the mid/high-q regime up to about 40 °C. At 40 °C, a gel profile evolves in the scattered intensity pattern for the PLGA-PEG_{1500}-PLGA system (cf. Figure 11). The hypothesis is that at this temperature the thermal energy is sufficiently high to break up the stable micellar structure and allowing one of the PLGA blocks of a chain to occupy a neighbor micelle and gradually forming an interconnected gel-network structure. We may note that the SANS patterns of the two samples at 30 and 50 °C have similar shape; hence also the copolymer with a long PEG-spacer exhibits rod-like conformation beyond the gel temperature. The scattered intensity is strongly reduced for also the PLGA-PEG_{1500}-PLGA sample at very high temperatures (70 °C) due to sedimentation of material.

These results show that the two polymer samples produce similar type of nanostructures over a broad temperature interval, but that the corresponding transitions on the nanoscale are shifted substantially to higher temperature for the copolymer with long PEG-spacer.

4. Conclusions

Biodegradable PLGA-PEG_n-PLGA triblock copolymers were synthesized by using ROP. In this work, the length of the hydrophobic PLGA block was kept constant, whereas the length of the hydrophilic PEG block was altered (n = 1000 and n = 1500). This variation is shown to have a pronounced impact on the phase behavior of the aqueous samples and the structure of the polymer both for dilute and semidilute samples. In dilute solution, the SANS profiles on the copolymer with short PEG-block yield asymmetric (ellipsoid) shapes, whereas the scattered intensity profile for the copolymer with n = 1500 can be modeled by a spherical core–shell model. The turbidity and viscosity measurements on dilute solutions of the copolymers suggest that loose intermicellar structures are formed upon an initial temperature increase, followed by contraction of the species and disintegration to micelles at higher temperatures. A similar pattern of behavior is observed for both copolymers, but the features occur at much higher temperatures for the copolymer with long PEG-spacer.

SANS experiments in the semidilute concentration regime of the copolymers, reveal a correlation peak at intermediate q values that suggests ordered structures with a characteristic intermicellar distance. In the gel region the correlation peak disappears and a less organized structure appears. At higher temperature, a cylindrical structure is established and at still higher temperatures packing of cylinders in a disordered way occurs. The main features are the same for both copolymers, the difference being that the observed features for the copolymer with n = 1500 are shifted to higher temperatures. The estimated complex viscosity suggests that the gel-network is transformed to a transient network at higher temperatures. This systematic survey of the structure of the copolymers at various temperatures and concentration regimes is important for proper formulation of systems for drug delivery and tissue engineering.

Supporting Information

Supporting Information is available from the Wiley Online Library or from the author.

Acknowledgements: B.N. acknowledges funding from the Norwegian Financial Mechanism 2009–2014 under Project Contract No. MSMT-28477/2014, Project No. 7F14009. B.N. appreciates the financial support of the European Union through the NanoS3 project (Grant No. 290251) of the FP7-PEOPLE-2011-ITN call. B.N. is grateful to Prof. Grijpma and Prof. Lendlein for the invitation to contribute with an article to an upcoming special issue in Macromolecular Bioscience.

Received: July 6, 2016; Revised: August 19, 2016; Published online: October 14, 2016; DOI: 10.1002/mabi.201600277

Keywords: ellipsoidal structures; hydrogels; SANS; temperature responsive triblock copolymer; transition to cylindrical structures

[1] P. Alexandridis, *Curr. Opin. Colloid Interface Sci.* **1996**, *1*, 490.
[2] I. W. Wyman, G. Liu, *Polymer* **2013**, *54*, 1950.
[3] J.-F. Gohy, *Block Copolymers II*, (Ed: V. Abetz), Springer, Berlin Heidelberg **2005**, pp. 65–136.
[4] C. Zhou, M.A. Hillmyer, T.P. Lodge, *Macromolecules* **2011**, *44*, 1635.
[5] S. Bayati, K. Zhu, L. T. T. Trinh, A.-L. Kjøniksen, B. Nyström, *J. Phys. Chem. B.* **2012**, *116*, 11386.
[6] M. A. Behrens, M. Lopez, A. L. Kjøniksen, K. Zhu, B. Nyström, J. S. Pedersen, *Langmuir* **2012**, *28*, 1105.
[7] A. Bajpai, S. K. Shukla, S. Bhanu, S. Kankane, *Prog. Polym. Sci.* **2008**, *33*, 1088.
[8] B. V. Slaughter, S. S. Khurshid, O. Z. Fisher, A. Khademhosseini, N. A. Peppas, *Adv. Mater.* **2009**, *21*, 3307.
[9] A. S. Hoffman, *Adv. Drug Delivery Rev.* **2012**, *64*, 18.
[10] C. M. Kirschner, K. S. Anseth, *Acta Mater.* **2013**, *61*, 931.
[11] Y. L. Cao, A. Rodriguez, M. Vacanti, C. Ibarra, C. Arevalo, C. A. Vacanti, *J. Biomater. Sci., Polym. Ed.* **1998**, *9*, 475.
[12] E. Ruel-Gariepy, J. C. Leroux, *Eur. J. Pharm. Biopharm.* **2004**, *58*, 409.
[13] D. Cohn, G. Lando, A. Sosnik, S. Garty, A. Levi, *Biomaterials* **2006**, *27*, 1718.
[14] S. Miyazaki, Y. Ohkawa, M. Takada, D. Attwood, *Chem. Pharm. Bull.* **1992**, *40*, 2224.
[15] R. Bhardwaj, J. Blanchard, *J. Pharm. Sci.* **1996**, *85*, 915.
[16] E. V. Batrakova, A. V. Kabanov, *J. Controlled Release* **2008**, *130*, 98.

[17] J. G. W. Wenzel, K. S. S. Balaji, K. Koushik, C. Navarre, S. H. Duran, C. H. Rahe, U. B. Kompella, *J. Controlled Release* **2002**, *85*, 51.
[18] J. S. Ahn, J. M. Suh, M. Y. Lee, B. Jeong, *Polym. Int.* **2005**, *54*, 842.
[19] B. Jeong, Y. H. Bae, S. W. Kim, *Macromolecules* **1999**, *32*, 7064.
[20] B. Jeong, S. W. Kim, Y. H. Bae, *Adv. Drug Delivery Rev.* **2002**, *54*, 37.
[21] L. Yu, J. Ding, *Chem. Soc. Rev.* **2008**, *37*, 1473.
[22] M. H. Park, H. K. Joo, B. G. Choi, B. Jeong, *Acc. Chem. Res.* **2011**, *44*, 72.
[23] G. M. Zentner, R. Rathi, C. Shih, J. C. McRea, M.-H. Sea, H. Oh, B. G. Rhee, J. Mestecky, Z. Moldoveanu, M. Morgan, S. Weitman, *J. Controlled Release* **2001**, *72*, 203.
[24] R. Rathi, G. M. Zentner, B. Jeong, *US Patent 6,201,072 B1*, **2001**.
[25] J. Bandrup, E. H. Immergut, E. A. Grulke, A. Abe, D. R. Bloch, *Polymer Handbook*, 4th ed., John Wiley & Sons, Inc., New York **1999**.
[26] H. Qian, A. R. Wohl, J. T. Crow, C. W. Macosko, T. R. Hpye, *Macromolecules* **2011**, *44*, 7132.
[27] A. L. Kjøniksen, A. Laukkanen, C. Galant, K. D. Knudsen, H. Tenhu, B. Nyström, *Macromolecules* **2005**, *38*, 948.
[28] R. Pamies, K. Zhu, A. L. Kjøniksen, B. Nyström, *Polym. Bull.* **2009**, *62*, 487.
[29] A. L. Kjøniksen, K. Zhu, M. A. Behrens, J. S. Pedersen, B. Nyström, *J. Phys. Chem. B* **2011**, *115*, 2125.
[30] S. Tanodekaew, J. Godward, F. Heatley, C. Booth, *Macromol. Chem. Phys.* **1997**, *198*, 3385.
[31] T. Riley, C. R. Heald, S. Stolnik, M. C. Garnett, L. Illum, S. S. Davis, S. M. King, R. K. Heenan, S. C. Purkiss, R. J. Barlow, P. R. Gellert, C. Washington, *Langmuir* **2003**, *19*, 8428.
[32] M. J. Park, K. Char, *Langmuir* **2004**, *20*, 2456.
[33] J. Chen, M. Liu, H. Gong, Y. Huang, C. Chen, *J. Phys. Chem. B* **2011**, *115*, 14947.
[34] N. Beheshti, K. D. Knudsen, K. Zhu, A.-L. Kjøniksen, B. Nyström, *Soft Matter* **2011**, *7*, 1168.
[35] A. Matsuyama, F. Tanaka, *Phys. Rev. Lett.* **1990**, *65*, 341.
[36] P.-G. de Gennes, *C. R. Acad. Sci. Paris Ser. II* **1991**, *313*, 1415.
[37] P. C. Painter, L. P. Berg, B. Veytsman, M. M. Coleman, *Macromolecules* **1997**, *30*, 7529.
[38] O. V. Borisov, A. Halperin, *Macromolecules* **1999**, *32*, 5097.
[39] K.-W. Kwon, M. J. Park, H. Kim, Y. H. Bae, K. Char, *Polymer* **2002**, *43*, 3353.
[40] M. J. Park, K. Char, *Langmuir* **2004**, *20*, 2456.
[41] B. Cabane, K. Lindell, S. Engström, B. Lindman, *Macromolecules* **1996**, *29*, 3188.
[42] N. S. Othman, M. S. Jaafar, A. A. Rahman, E. S. Othman, A. A. Rozlan, *Int. J. Biosci. Bioinf.* **2011**, *1*, 223.
[43] F. Tanaka, M. Ishida, *Macromolecules* **1996**, *29*, 7571.
[44] F. Tanaka, W. H. Stockmayer, *Macromolecules* **1994**, *27*, 3943.
[45] A. N. Semenov, M. Rubinstein, *Macromolecules* **1998**, *31*, 1373.
[46] F. Tanaka, *Polymer Physics: Applications to Molecular Association and Thermoreversible Gelation*, Cambridge University Press, UK **2011**.
[47] G. Chang, L. Yu, Z. Yang, J. Ding, *Polymer* **2009**, *50*, 6111.
[48] L. Chen, T. Ci, L. Yu, J. Ding, *Macromolecules* **2015**, *48*, 3662.
[49] P. Zou, J. Suo, L. Nie, S. Feng, *Polymer* **2012**, *53*, 1245.
[50] S. J. Lee, C. W. Park, S. C. Kim, *Polym. J.* **2009**, *41*, 425.
[51] A. Kermagoret, C.-A. Fustin, M. Bourguignon, C. Detrembleur, C. Jerome, A. Debuigne, *Polym. Chem.* **2013**, *4*, 2575.
[52] B. Zhang, H. Tang, P. Wu, *Macromolecules* **2014**, *47*, 4728.
[53] Y. G. Jia, X. X. Zhu, *Polym. Chem.* **2014**, *5*, 4358.
[54] F. Kafer, F. Y. Liu, U. Stahlschmid, V. Jerome, R. Freitag, M. Karg, S. Agarwal, *Langmuir* **2015**, *31*, 8940.
[55] H. Tanaka, *Macromolecules* **1992**, *25*, 6377.
[56] G. Raos, G. Allegra, *Macromolecules* **1996**, *29*, 6663.
[57] S. Picarra, J. M. G. Martinho, *Macromolecules* **2001**, *34*, 53.
[58] H. H. Winter, F. Chambon, *J. Rheol.* **1986**, *30*, 367.
[59] D. F. Hodgson, E. J. Amis, *J. Non-Cryst. Solids* **1991**, *131*, 913.
[60] M. Muthukumar, *Macromolecules* **1989**, *22*, 4656.
[61] S. R. Kline, *J. Appl. Cryst.* **2006**, *39*, 895.
[62] ftp://ftp.ncnr.nist.gov/pub/sans/kline/Download/SANS_Model_Docs_v4.10.pdf
[63] L. Yu, G. Chang, H. Zhang, J. Ding, *J. Polym. Sci., Part A* **2007**, *45*, 1122.
[64] H. Zhang, L , Yu, J. Ding, *Macromolecules* **2008**, *41*, 6493.
[65] B. A. Simmons, G. C. Irvin, V. Agarwal, A. Bose, V. T. John, G. L. McPherson, N. P. Balsara, *Langmuir* **2002**, *18*, 624.
[66] M. J. Park, K. Char, J. Bang, T. P. Lodge, *Langmuir* **2005**, *21*, 1403.
[67] J. E. Martin, D. Adolf, *Annu. Rev. Phys. Chem.* **1991**, *42*, 311.
[68] D. S. Lee, M. S. Shim, S. W. Kim, H. Lee, I. Park, T. Chang, *Macromol. Rapid Commun.* **2001**, *22*, 587.
[69] L. Yu, Z. Zhang, H. Zhang, J. Ding, *Biomacromolecules* **2009**, *10*, 1547.